Nuclear Medicine & Radiation Therapy

Johansson et al., J Nucl Med Radiat Ther 2014, 5:1
http://dx.doi.org/10.4172/2155-9619.1000171

Research Article Open Access

A Biologically Conformal Intensity-Modulated Radiotherapy Framework Based on [18F] Fluoro-Deoxy-Glucose Positron Emission Tomography for Individualized Cancer Treatment

Annelie Johansson[1], Camilo J. Sanz Freire[2], Pedro M. Collado Chamorro[2], Susana Pérez Echagüen[3], Gustavo A. Ossola Lentati[3] and Alejandro Sánchez-Crespo[1*]

[1]*Department of Hospital Physics, Karolinska University Hospital, Stockholm, Sweden*

[2]*Department of Medical Physics, Centre for Biomedical Research of La Rioja, Spain*

[3]*Department of Radiation Oncology, Centre for Biomedical Research of La Rioja, Spain*

[*]**Corresponding author:** Alejandro Sánchez-Crespo, Associate Professor, Department of Nuclear Medicine Karolinska University Hospital, S-171 76 Stockholm, Sweden, Tel: +46851779315; E-mail: alejandro.sanchez-crespo@karolinska.se

Received date: Mar 27, 2014, **Accepted date:** April 21, 2014, **Publication date:** April 30, 2014

Abstract

Purpose: To develop a framework for biologically-optimized routine intensity modulated radiotherapy (IMRT) treatment plans based on 18F-fluoro-deoxy-glucose (FDG)-Positron Emission Tomography (PET)/Computed Tomography imaging.

Methods and materials: The dose-planning FDG-PET images are first corrected for partial volume effect using an iterative algorithm with a noise suppression filter. Thereafter, the FDG-uptake is used for transforming the delineated clinical target volume (CTV) into a set of biological planning target volumes (bPTV). This is done with an optimization algorithm that groups pixel values with the objective of maximizing the FDG-uptake variance between bPTV. The resulting average FDG pixel intensity within each bPTV, together with a tumor control probability (TCP) function, are used to obtain the prescribed dose to each bPTV that maximize the total TCP, using dose limits to the organs at risk (OAR) as constraints. The accuracy of this method was tested on a phantom. Additionally, this framework was also tested on five patients with head-neck cancer, in a retrospective clinical trial.

Results: The extension of the obtained bPTV and their activity concentration showed good agreement with the true FDG distribution in the phantom. All patients planned using the presented methodology achieved a notable increase in TCP, compared to the standard IMRT plans.

Conclusions: FDG-PET together with this framework can be used to biologically optimize IMRT to individualize cancer treatment.

Keywords: FDG; PET/CT; IMRT; biological optimization; individualized cancer treatment; TCP

Introduction

The evolution of radiotherapy (RT) from 3-dimentional conformal RT using forward dose planning to intensity modulated radiotherapy (IMRT) using inverse dose planning has yielded great possibilities for producing highly conformal dose distributions. This development is proving its importance due to the fact that a tumor is not a homogeneous mass in terms of radiosensitivity, hence neither should radiation dose be homogeneous. Biological properties affecting the radiosensitivity of the tumor can be studied in a non-invasive manner using functional imaging. The incorporation of such information into treatment planning is thus considered the future of individualized IMRT optimization. A commonly used functional imaging technique is Positron Emission Tomography (PET) using 18F-Fluoro-Deoxy-Glucose (FDG). FDG is a glucose analog with increased uptake in areas of elevated metabolic rate. Aside from normal uptake in active organs, clonogenic cells are known to have a high rate of glucose consumption. This enables differentiating actual clonogenic cells from tumor mass as seen by computed tomography (CT). Although a vast number of factors affect the uptake of FDG in a tumor, a linear relation between the uptake and clonogenic cell density is the more plausible hypothesis. This has been supported by experimental evidence in a number of different cell types both by *in-vitro* [1-3] and *in-vivo* [4-8] experiments. Furthermore, it has been demonstrated that the majority of tumor recurrences after completed RT appears in regions of high FDG-uptake on the pre-treatment scan. This has been shown both in head and neck cancer (HNC) [9-11] and in non-small cell lung cancer (NSCLC) [12,13]. Furthermore, it has been shown that the density of relapses increases with increasing PET standardized uptake value [11]. Another study showed that the location of the low and high FDG-uptake areas remains stable throughout the course of RT when delivering a homogeneous dose to NSCLC [14]. All together, these findings stress the possible gain of modeling the dose according to the distribution and level of FDG-uptake.

Different methods have been proposed (and in some cases implemented) using biological information attained from PET images for improving RT treatment plans. The different methods can roughly be divided into three major concepts, namely boost dosage, dose painting by contours (DPBC) and dose painting by numbers (DPBN).

The first mentioned is already in common use in clinical practice and involves delineation of one or a small number of target subvolumes, which are treated with a higher dose compared to the rest of the target [9]. The delineation of the subvolumes is performed either visually from the PET images or using an algorithm, often related to the maximum standardized uptake value (SUVmax) in the tumor [15]. The dosage is prescribed by a radiation oncologist and consists of standardized values based on clinical experience. In dose painting the PET images are used in a more quantitative manner, converting image intensities into an inhomogeneous dose prescription map. The difference between DPBC and DPBN lies in that in DPBC the dose levels are discretized by dividing the target volume into a number of subvolumes according to the level of tracer uptake [16]. On the other hand, in DPBN the dose levels are continuous in the sense that each voxel receives its own individual dose prescription [17-19]. To this day dose painting with FDG-PET has only been attempted using linear function, relating image intensities and prescribed dose. To our knowledge this is an approach that has not been justified by any radiobiological or radiopharmaceutical model. Furthermore, this approach does not take into account other physical factors, like the presence of organs at risk (OARs) and dose conformality, for creating an optimal dose distribution that maximize tumor control probability (TCP). Yang and Xing did however show a theoretical framework for prescribing doses based on a TCP model and radiosensitivity parameters that could hypothetically be derived from functional imaging [20]. However, they did not possess knowledge on how to obtain these parameters from real functional images. Another detail that seems to have been neglected in past dose painting approaches is the well known problem of partial volume effect (PVE) which heavily impairs PET tracer quantification. PVE in PET occurs because of the positron range, the annihilation photon depth of interaction in the detector crystals, the incorrect sampling of coincidence lines between detector units, the a-collinear emission of the annihilation photons and the finite size of the PET detector units [21,22]. PVE causes both spatial and quantitative degradation of the PET images by smearing out the voxel intensities [23]. As DPBN brings upon more dose conformality than DPBC, it could be considered the technique of choice. However DPBN also brings an unprecedented source of geometrical uncertainties to the treatment. These must be addressed thoroughly before DPBN can be used in clinical routine. Fortunately studies comparing DPBN with DPBC suggest that with the appropriate delineation and dose level selection, DPBC might produce equal or even superior TCP [24,25].

In this paper we aim to bring together the current knowledge on quantitative PET image processing, FDG uptake in cancerous tissue and strategies for biological RT optimization including TCP optimization. The product is a general practical-framework, for incorporating FDG-PET/CT imaging into the biological optimization of IMRT treatment planning, applicable to the clinical routine practice.

Materials and Methods

Framework

Following is a step by step chronological description of the proposed practical framework for biological optimization of IMRT plans based on FDG-PET/CT. The starting point is a set of dose planning FDG PET/CT simulation images.

PET image partial volume correction: The dose-planning FDG-PET images are first corrected for PVE. The partial volume correction (PVC) method used in this work converges towards the true image by iteratively minimizing the second term in Eq (1)

$$O(x,y,z)^{k+1} = O(x,y,z)^{k} + \alpha\left(I(x,y,z) - O(x,y,z)^{k} \otimes PSF(x,y,z)\right) \quad (1)$$

where $O(x,y,z)^k$ is the k:th estimate of the true FDG distribution at position (x,y,z) in the image, I(x,y,z) is the original image intensity (corrected for photon attenuation and scattering, random coincidences and sensitivity variations), α a convergence parameter, PSF is the point spread function of the used PET scanner and ⊗ denotes convolution operation. A bilateral filter [26] is applied after each iteration step to reduce the noise amplification derived from the convolution operator.

Definition of Biological planning target volumes: The radiation oncologists delineate the clinical target volume (CTV) on the CT scan, based on the spatial distribution of the PVC-FDG uptake. In this way the segmentation reflects the variability within the tumor volume.

The FDG-intensity values within the entire CTV are used to produce a number of clusters representing similar biological properties. This segmentation is performed using the method presented by Otsu 1979 [27]. The starting point is to define the number of clusters to be achieved, with the premise of grouping pixels representing similar biological properties. The number of possible clusters should be defined considering both the actual volume of the initial CTV and the disadvantages of using a large number of biological targets (due to geometrical mismatch, tumor dynamics and dose delivery complexity). The Otsu´s method uses then the FDG pixel value histogram within the considered CTV and the desired number of clusters to calculate the optimal pixel value threshold(s) which maximizes the inter-cluster- and minimizes the intra-cluster pixel value variance. The boundaries of the initial CTV now correspond to the outer borders of the clusters. Due to positioning uncertainties margins are added to these outer borders of each respective cluster, creating the final biological Planning Target Volumes (bPTV). The entire volume to be treated is thus now composed of bPTV.

Dose prescription to the bPTV: In the final step of this framework, the FDG-PET pixel intensities within each cluster are used to derive a dose prescription to each bPTV. The dose prescription will maximize the total tumor TCP using the imposed dose limits to the OARs as constraints

$$TCT_{tot} = \prod_{j=1}^{L} TCP_j \quad (2)$$

where L is the number of bPTV and the function describing each TCPj is modeled according to the well known radiobiological model proposed by Nahum and Sanchez-Nieto 2001 [28].

$$TCP_j = \int_0^{\infty} \frac{e^{\frac{-(\alpha-\bar{\alpha})^2}{2\sigma_\alpha^2}}}{\sigma_\alpha\sqrt{2\pi}} \exp[-\rho_j V_j \cdot \exp(-\alpha \cdot D_j(1+\frac{\beta}{\alpha} \cdot d_j))]\, d\alpha$$

(3)Where α and β are tumor-specific radiosensitivity parameters and D_j, d_j, V_j and ρ_j are the total dose, the specific fraction dose, the volume and the clonogenic cell density for $bPTV_j$, respectively. The parameter α follows a Gaussian distribution with mean $\bar{\alpha}$and standard deviation σ_α.. The average FDG-PET image activity concentration in a given bPTVj is used to estimate ρ_j by using the linear relationship between clonogenic cellular density and FDG uptake established by Fischer et al, 2006 [1]. Once the set of parameters ($\bar{\alpha}, \sigma_\alpha, \beta, \rho_j, V_j$) in Eq. (3) are defined for each $bPTV_j$, a 95% initial objective TCP ($TCP_{Objective}$) is used to obtain the set of prescribed doses D_j with j=1,…,L) that minimizes the function;

$TCP_{Objective} - TCP_{Total}(D_j)$ (4) As an example, Figure 1 shows all possible combinations of prescribed doses for a target with two hypothetical bPTVs producing the same TCPTotal as a function of different dose fractionations. From this set of prescribed doses Dj($TCP_{Objective}, \bar{\alpha}, \sigma_\alpha, \beta, \rho_j, V_j$), the combination for which doses among bPTVs are equal (classical case) is initially selected. This together with the anatomical CT images and the set of RT structures (including bPTV) are used in a standard physical IMRT optimization process. The resulting isodose distribution is analyzed with regards to OAR involvement. If the OAR dose limits are surpassed a new combination of prescribed doses are chosen from the set $D_j$and the physical IMRT optimization repeated. If none of the possible D_j combinations for the considered level of TCPtot are feasible with respect to OAR dose limits, the process is iteratively repeated by decreasing the value of $TCP_{Objective}$. The general layout of this work is described in (Figure 2).

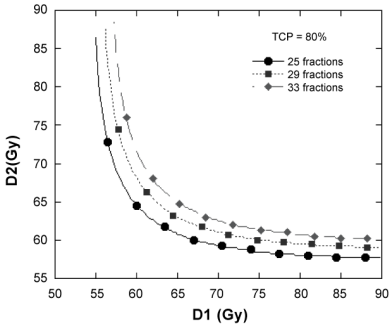

Figure 1: Example of dose prescription, D1 and D2 for two hypothetical biological planning target volumes (bPTV) producing uniform level of tumor control probability (TCP) as a function of number of fractions. Calculation performed using Eq. (3-4) with TCP_{init}=80%, α=0.3Gy-1, σ_α=0.069Gy-1, α/β=10.5Gy and $bPTV_1$ with V_1=21.3 ml, ρ_1=0.5 cells/m_l and $bPTV_2$ with V_2=2.8 ml, ρ_2=1.4 cells/ml.

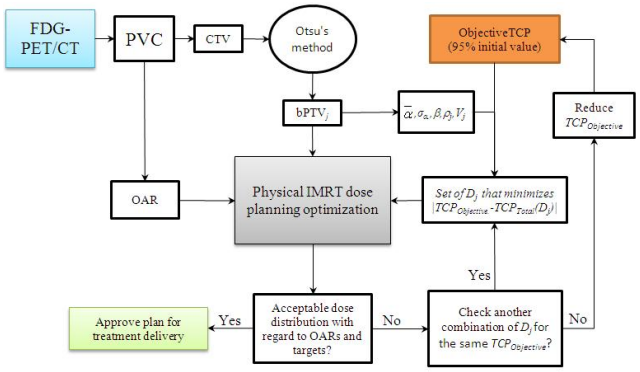

Figure 2: Flowchart showing the iterative method for biologically optimization of the intensity modulated radiotherapy (IMRT) plan described in this work. The initial FDG-PET images are corrected for partial volume (PVC) effect prior definition of the clinical target volume (CTV) and organs at risk (OAR). Thereafter, the Otsus´s method is used to segment the CTV into "j" biological planning target volumes ($bPTV_j$). Dose prescription to each target volume (D_j) is based on the FDG uptake and a tumor control probability (TCP) model. See the main text for a description of the parameters $\bar{\alpha}, \sigma_\alpha, \beta, \rho_j$ and V_j .

Methodological validation

A phantom consisting of three concentric cylinders of radius 1.5, 3 and 4.5 cm was used to test the accuracy of the PVC and the segmentation algorithm used in this framework. Each cylinder was filled with different concentrations of FDG (8.14, 13.57 and 25.35 kBq/ml, respectively) and placed within a water-filled container simulating a body. The phantom was scanned in a Biograph 64 PET/CT scanner (Siemens Medical Solutions, Concord, CA), with 2D-OSEM reconstruction (4 iterations, 8 subsets and a 5_{mm} Gaussian filter). Corrections were applied for activity decay, photon attenuation and scatter, random coincidences, detector sensitivity variations and partial volume effect. The resulting PET/CT images were then transferred into an ECLIPSE treatment planning system (Varian Medical, Palo Alto, CA). The outer cylinder of the phantom was then delineated using the CT images in order to create an initial RT-structure set consisting on a single CTV. The PVC algorithm together with the segmentation method previously described, were then used in the FDG-PET images of the phantom to generate three clusters corresponding to the three inner cylinders of the phantom. The extension of these clusters and their activity concentration were compared to the real extension of the cylinders and their initial activity concentration.

Clinical implementation of the method

This framework was tested retrospectively on five patients with known head and neck cancer (HNC). Treating HNC is generally subject to a high geometrical complexity with regards to the closely adjacent OARs and often large tumor volume involvement. The patients underwent a FDG-PET/CT scan for RT dose planning simulation and treated with routine 3D-conformal RT. PET/CT simulation was performed in a Biograph 6 PET/CT scanner (Siemens

Medical Solutions) in supine position, using a head, neck and shoulder IMRT-specific thermoplastic mask. Slice thickness was set to 2.5 mm.

In order to test the clinical applicability of the presented framework, two competing IMRT plans were created for each patient, both using as starting point the originally delineated CTV. The first IMRT plan, standard-plan, is based on the CTV, PTV and doses prescribed by radiation-oncologist, i.e. physical optimization. The other IMRT plan, Biop-plan, is optimized according to the method presented in this work using a conservative number of bPTV set to two for all patients. Both IMRT plans share the same standard dose limits to OAR (Table 1) and radiosensitivity parameters (α=0.3Gy-1, $\sigma\alpha$=0.069Gy-1, α/β=10.5Gy) [29-31]. For simplification no accelerated proliferation was considered but could be easily included in the methodology and will be considered in future developments. An approximate of the clonogenic cell density in each target volume was calculated using the linear relationship established by Fischer et al. 2006 for small cell lung cancer (SCLC), 0.003 Bq per cell [1].

Organ	Dose limits [Gy]	Reference
Thyroid	D_{mean}< 45	[33]
Mandible	D_{33}<65 D_{66}<60 D_{100}< 60 for TD_5/5	[33]
Eyes, each	D_{max} < 35	[33]
Lens of eye, each	D_{max} < 5-8	[33]
Parotid gland	D_{mean} < 25	[34]
Brainstem	D_{max} < 54	[34]
Medulla, extended 3 mm	D_{max} < 45	[34]
Heart	D_{mean}< 26 V30Gy<46%	[34]
Esophagus	D_{mean}<34	[34]
Lungs	V20Gy<20% D_{mean}≤20-23	[34]

Table 1: Dose limits for organs at risk (OARs) used in this study.

Where D_x= x% of the total volume receiving a given dose and VxGy=Volume of organ that receives the dose limit x

A class solution was applied consisting of nine equally spaced multi leaf collimator fields starting at 180º, 6 MV photon energy and isocenter set at the center of mass of the total target volume. IMRT physical optimization was performed using Dose Volume Optimizer 11.0.30 (Varian Medical) and the dose calculation was performed using Anisotropic Analytical Algorithm version 11.0.30 (Varian Medical) with a grid size of 0.25 cm. The prescribed doses were considered achieved when received by more than 95% of the target volume. Standard-plans and Biop-plans were compared in terms of achieved total TCP and doses to OAR, using the BioSuite software [32]. BioSuite handles one RT-structure at a time and uses the dose volume histogram (DVH) to calculate the TCP with the radiosensitivity parameters and the calculated clonogenic cell density specific to each bPTV, whereon total TCP is calculated by Eq. (2).

Results

Methodological validation

(Figure 3) shows that the dimensions of the calculated clusters on the FDG-PET images are in good accordance with the real values of the three phantom compartments. The obtained activity concentration (kBq/ml) in each compartment was 10.2, 14.3 and 20.7 from the inner compartment and out, respectively.

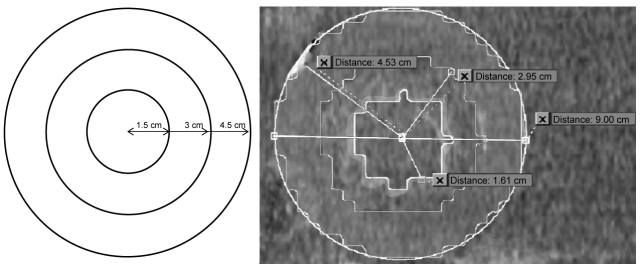

Figure 3: To the left, cross-section of the phantom. Indicated, the dimensions for each compartment. To the right, the corresponding PET/CT image after partial volume correction and segmentation. Indicated the resulting dimensions.

Clinical implementation of the method

Figure 4 shows the standard PTV (created from the initial CTV) and the corresponding bPTV, as an example of the clinical implementation of this framework in one HNC patient.

Table 2 shows that, without surpassing the maximum dose to the OARs, all patients planned using Biop-plan achieved a notable increase on their TCP, which was not reached with the standard IMRT plans.

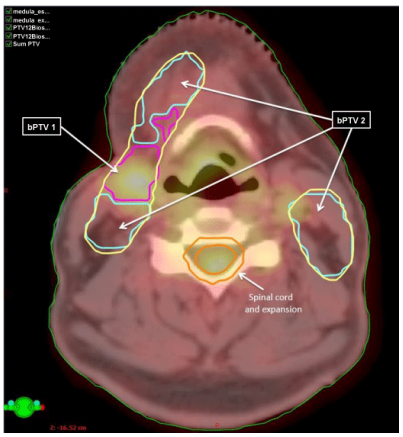

Figure 4: Fused FDG-PET/CT transversal section of a clinical head and neck cancer patient. Delineated, initial clinical target volume (yellow) and the corresponding biological planning target volumes based on the distribution of FDG-PET/CT (blue and magenta). Organs at risk are spinal cord and expansion (orange).

Patient #	Diagnosis	Dose prescribed		No. of fractions	OAR doses [Gy]			TCP	
		Standard-plan	Biop-plan		Organs	Standard-plan	Biop-plan	Standard-plan	Biop-plan
1	Primary tumor: Carcinoma of naso-pharynx	PTV1: nasopharynx + prophylactic dose to first two levels of lymph node change, 21.6 Gy	bPTV 1: 60.5 Gy, 96% of total target volume (PTV1), 0.57·104 Bq/ml§	28	Eye, right (max):	2.8	2.8	46.3%	74.0%
					Eye, left (max):	2.5	2.4		
					Thyroid (mean):	0.9	1.0		
					Mandible* (max):	D33:46.6 D66:34.5 D100: 60.5	D33:43.4 D66:37.0 D100: 61.6		
	Secondary tumor: Cervical lymphadeno pathy	PTV2: boost to nasopharynx (PTV2 PTV1), 50.4 Gy	bPTV 2: 75 Gy, 4% of total target volume, 1.42·104 Bq/ml§		Spinal cord (max):	44.6	44.1		
					Parotid, right (mean):	24.3	25.9		
					Parotid, left (mean):	24.4	25.4		
					Brainstem (max):	53.1	50.5		
2	Epidermoidal carcinoma of the vocal cord, larynx. Moderately differentiated	PTV1: all of tumor and prophylactic dose to cervical nodules, 45 Gy	bPTV 1: 63 Gy, 64% of total target volume (PTV1), 1.85·103 Bq/ml§	25	Eye, right (max):	1.1	1.5	14.4%	67.6%
					Eye, left (max):	1.1	1.4		
					Thyroid* (mean):	27.0	32.4		
	.	PTV2: boost to positive cervical nodules and tumor (PTV2 PTV1), 10 Gy	bPTV 2: 69.75 Gy, 36% of total target volume, 4.67·103 Bq/ml§		Mandible* (max):	D33:36.8 D66:30.2 D100:52.0	D33:51.1 D66:40.0 D100:80.9		
					Spinal cord (max):	44.7	44.5		
					Parotid, right (mean):	23.6	23.2		
		PTV3: boost to tumor (PTV3 PTV2), 14 Gy			Parotid, left (mean):	24.1	23.4		
					Brainstem (max):	45.7	51.3		
3	Carcinoma of oro-pharynx, oral cavity. Moderately differentiated and positive nodes on right side. Had surgery however dose prescribed is radical.	PTV1: tumor volume, 54 Gy	bPTV 1: 77 Gy, 70% of total target volume (PTV1 PTV2 PTV3), 1.96·103 Bq/ml§	30	Eye, right (max):	0.8	1.0	28.3%	91.2%
					Eye, left (max):	0.7	0.9		
					Thyroid* (mean):	9.7	11.1		
					Mandible* (max):	D33:37.2 D66:17.6 D100:59.2	D33:40.3 D66:21.2 D100:76.6		
		PTV2: right nodes, 60 Gy	bPTV 2: 70.5 Gy, 30% of total target volume, 4.61·103 Bq/ml§		Spinal cord (max):	41.9	43.0		
		PTV3: left nodes prophylactic dose, 46 Gy			Parotid, right (mean):	10.0	12.72		
					Parotid, left (mean):	6.3	8.8		
					Brainstem (max):	1.8	2.3		

4	Glottis carcinoma, larynx. Moderately differentiated with primary tumor on right vocal cord, secondary on left vocal cord. Necrosis in center of tumor. No prophylactic dose to lymph nodes because of high age.	PTV: 70 Gy	bPTV 1: 73 Gy, 98% of total target volume (PTV), 0.80·104 Bq/ml§	35	Eye, right (max):	0.2	0.2	75.5%	83.2%
					Eye, left (max):	0.2	0.2		
					Thyroid* (mean):	25.1	27.0		
			bPTV 2: 78.25 Gy, 2% of total target volume, 5.89·104 Bq/ml§		Mandible (max):	D33:0.9 D66:0.6 D100:21.4	D33:1.0 D66:0.6 D100:22.8		
					Spinal cord (max):	43.1	43.1		
					Parotid, right (mean):	0.4	0.4		
					Parotid, left (mean):	0.5	0.5		
5	Supraglottis carcinoma, poorly differentiated and bilateral cervical positive	PTV1: primary tumor and cervical nodes, 50.4 Gy	bPTV 1: 61.5 Gy, 61% of total target volume (PTV1), 2.51·103 Bq/ml§	28	Eye, right (max):	2.0	2.2	22.2%	31.7%
					Eye, left (max):	2.0	2.2		
					Thyroid*(mean):	45.4	55.8		
		PTV2: boost to primary tumor (PTV2 PTV1), 16 Gy	bPTV 2: 65.5 Gy, 39% of total target volume, 5.19·103 Bq/ml§		Mandible * (max):	D33:48.4 D66:38.5 D100:70.2	D33:50.0 D66:35.4 D100:100.0		
					Spinal cord (max):	43.5	44.9		
					Parotid, right (mean):	31.2	24.5		
					Parotid, left* (mean):	36.6	22.9		

Table 2: Patient diagnosis, dose prescriptions, number of fractions, doses reached for organs at risk (OAR), and final achieved tumor control probability (TCP) for the physically optimized IMRT plan (standard-plan) and the biologically optimized IMRT plan (Biop-plan) in all patients considered in this study. *Organ at risk partly included in target volume ; Dx: x% of the total volume receives the given dose

Generally, all but one patient received the larger dose to the bPTV with the higher FDG-uptake (Table 2). For patient 3, the best combination of prescribed doses, which resulted in the highest TCP, was such that the bPTV with the highest FDG-uptake received the lower radiation dose. This paradoxical result was most likely due to two factors, the anatomical location of the bPTV (within OAR) and the small impact of ρ on the TCP.

Discussion and Conclusion

Compared to previously methodologies, the novelty of the presented framework lies on;

The use of an iterative PVC routine which results in improved quantitative properties of the FDG-PET images. The quality of the method heavily depends on two aspects; the spatial location of the bPTV and the accuracy in the calculation of dose prescription, both of which will in turn depend on corrections for PVE. To our knowledge, PVC has never been included in any of the previously reported dose painting approaches.

Compared to the commonly used percentage of the SUVmax method [15] for image segmentation, where the definition of the subvolumes depends heavily on both PVE and image noise, the Otsu´s method after PVC, ensures inclusion of the entire uptake distribution into the treatment plan.

The use of the FDG uptake to determine clonogenic cell density in each bPTV. Grouping homogeneous subvolumes in terms of clonogenic cell densities replaces the primitive assumption that the entire CTV is homogeneous.

Each level of TCP results in a range of possible prescribed dose combinations between bPTV (see for instance (Figure 1) for a two dimensional problem). Using this distribution in an iterative way the optimal dose prescription in each bPTV can be objectively obtained with respect to adjacent OARs. This dose method replaces population-based dose prescription, offering a biologically and physically individualized dose prescription. Furthermore it replaces the linear relationship established by many authors between FDG uptake and dose [16,17,19]. The potential impact of dose prescription based on TCP in conjunction with FDG, instead of using standard doses, is an interesting topic of discussion. The LQ-TCP model used in this paper has been, although in the shape of many small alterations, vastly proven sound both in vitro and in vivo environments. This model allows for some non-intuitive solutions, where a low dose in a high-uptake volume can be compensated by a high dose in a low-uptake

volume without altering the total TCP. This becomes useful when a dose in a volume is forced to be low due to an adjacent OAR (for instance in patient 3). But can this solution be trusted in the view of previous studies showing that tumor recurrence appears predominantly in tumor regions with initially high FDG uptake [9-13]? Considering that these studies were performed by investigating tumors which were treated with homogeneous dose to the entire tumor, it is then expected according to the LQ-TCP model that tumor regions with high tumor cell densities should have lower TCP value, resulting in more recurrences. Hence these studies are indeed not contradicting these non-intuitive possibilities in dose prescription based on the LQ-TCP model.

Limitations of the method and practical considerations: The ability of the proposed iterative PVC routine to recover the true FDG activity distribution is limited and depends strongly on both the size and its intensity level (Figure 3). The true activity concentration in small objects, close to the spatial resolution of the PET scanner, is more difficult to recover. This error is propagated to the calculation of clonogenic cell density. However, due to the dependence of TCPj with ρj (Eq. 3), this error has in general a small impact in the calculated dose prescription. Furthermore, despite of the many publications supporting a linear relationship between clonogenic cell density and FDG-uptake [1-8], specific values for head-neck cancer were not found in the literature. Hence in this work, all calculations were performed using the slope of the linear relation between FDG-uptake and SCLC [1]. Different tumor types, physiological conditions and PET camera specific values of this relation were intentionally left for future development.

The accuracy of published radiosensitivity values (α, β) can be highly debatable. In vivo studies are rare and relatively old (with the exception of prostate cancer), conducted with outdated treatment delivery and dose calculation techniques. In general similar studies resulted in different values due to the large inter-patient and intra-tumor heterogeneities, which reflect the difficulties in reaching a definite conclusion. As an example, the HNC study by Stuschke and Thames [31], which involved a large number of patients from five different trials, resulted in a spread of α/β values ranging from 6.5 to 27 Gy. Different authors use also different approximations of the LQ-model. For this reason, in clinical applications, it is sometimes necessary to combine radiosensitivity values from different publications.

In clinical practice, there is a tradeoff between the number of bPTV that can be defined and both, the complexity of the intended dose distribution and the geometrical uncertainties in delivering the radiation dose (due to hardware limitations and target location and dynamics). Additionally, to determine the dose prescription with this methodology for a large number of bPTV could be an ill posed problem. In the limit where the number of bPTV is equal to the number of pixels of the original CTV, we have the DPBN situation. This is a special case where the number of possible combinations of dose prescriptions becomes too large to be handled by the technique explained in this work.

When two bPTV, with prescribed doses D1 > D2 are adjacent to each other, a heavier weight should be given to the homogeneity constraint for the volume associated to D1 during dose planning. This will produce a dose gradient falling off at the lower dose side of the border between the two bPTV, accounting for some of the geometrical uncertainties of dose delivery.

In order for the prescribed dose plan to reach its curative intent the defined CTV have to include all clonogenic cells. This represents a challenge when using FDG and a single PET scan. In order to better discriminate the FDG uptake in clonogenic cells from normal cell uptake (like inflammatory processes), we suggest to perform a dynamic or a dual time point PET scan, rather than a single PET scan, to produce parametric PET images. In this way the kinetic differences in FDG uptake between normal and cancer tissues will ensure an optimal target and clonogenic cell definition.

Conclusion

The framework presented handles both the spatial location and the level of the radiation dose prescription, based on the patient specific biological properties derived from the FDG-PET images. Compared to the traditional approach of optimizing IMRT based on physical constrains, the presented biological IMRT optimization resulted in a significant TCP increase, without surpassing dose limits to the OARs, in all patients of the retrospective clinical trial. To our knowledge, this is the first time that the specific biological characteristics of the FDG uptake and partial volume corrected PET images are included in a TCP driven IMRT optimization approach. This framework will bring a new insight into the biological optimization of IMRT plans based on widespread FDG- PET imaging.

Conflict of Interest

There was no economical/personal relationship that could inappropriately influence this work.

Acknowledgments

This work was economically supported with a FoUU grant from the Department of Hospital Physics of the Karolinska University Hospital, Stockholm, Sweden.

References

1. Fischer BM, Olsen MW, Ley CD, Klausen TL, Mortensen J, et al. (2006) How few cancer cells can be detected by positron emission tomography? A frequent question addressed by an in vitro study. Eur J Nucl Med Mol Imaging 33: 697-702.
2. Higashi K, Clavo AC, Wahl RL (1993) Does FDG uptake measure proliferative activity of human cancer cells? In vitro comparison with DNA flow cytometry and tritiated thymidine uptake. J Nucl Med 34: 414-419.
3. Minn H, Clavo AC, Grénman R, Wahl RL (1995) In vitro comparison of cell proliferation kinetics and uptake of tritiated fluorodeoxyglucose and L-methionine in squamous-cell carcinoma of the head and neck. J Nucl Med 36: 252-258.
4. Herholz K, Pietrzyk U, Voges J, Schröder R, Halber M, et al. (1993) Correlation of glucose consumption and tumor cell density in astrocytomas. A stereotactic PET study. J Neurosurg 79: 853-858.
5. Higashi T, Tamaki N, Torizuka T, Nakamoto Y, Sakahara H, et al. (1998) FDG uptake, GLUT-1 glucose transporter and cellularity in human pancreatic tumors. J Nucl Med 39: 1727-1735.
6. Folpe AL, Lyles RH, Sprouse JT, Conrad EU 3rd and Eary JF (2000) (F-18) Fluorodeoxyglucose positron emission tomography as a predictor of pathologic grade and other prognostic variables in bone and soft tissue sarcoma. Clin Cancer Res. 6: 1279-1287
7. Bos R, van Der Hoeven JJ, van Der Wall E, van Der Groep P, van Diest PJ, et al. (2002) Biologic correlates of (18)fluorodeoxyglucose uptake in human breast cancer measured by positron emission tomography. J Clin Oncol 20: 379-387.

8. Dooms C, van Baardwijk A, Verbeken E, van Suylen RJ, Stroobants S, et al.(2009) Association between 18F-Fluoro-2-Deoxy-D-Glucose uptake values and tumor vitality: Prognostic value of positron emission tomography in early-stage non-small cell lung cancer. J Thoractic Oncology. 4 : 822-828
9. Madani I, Duthoy W, Derie C, De Gersem W, Boterberg T, et al. (2007) Positron emission tomography-guided, focal-dose escalation using intensity-modulated radiotherapy for head and neck cancer. Int J Radiat Oncol Biol Phys 68: 126-135.
10. Soto DE, Kessler ML, Piert M, Eisbruch A (2008) Correlation Between Pretreatment FDG-PET Biological Target Volume and Anatomical Location of Failure after Radiation Therapy for Head & Neck Cancers. Radiother Oncol. 89 :13-18
11. Due, Anne Kirkebjerg (2012) Recurrence location after definitive (chemo) radiation therapy for head and neck squamos cell carcinoma in relation to clinical target volumes and (18F)-FDG uptake. Copenhagen University Hospital. 65.
12. Aerts HJ, van Baardwijk AA, Petit SF, Offermann C, Loon Jv, et al. (2009) Identification of residual metabolic-active areas within individual NSCLC tumours using a pre-radiotherapy 18Fluorodeoxyglucose-PET-CT scan. Radiother Oncol. 91: 386-392
13. Abramyuk A, Tokalov S, Zöphel K, Koch A, Szluha Lazanyi K, et al. (2009) Is pre-therapeutical FDG-PET/CT capable to detect high risk tumor subvolumes responsible for local failure in non-small cell lung cancer? Radiother Oncol 91: 399-404.
14. Aerts HJ, Bosmans G, van Baardwijk AA, Dekker AL, Oellers MC, et al. (2008) Stability of 18F-deoxyglucose uptake locations within tumor during radiotherapy for NSCLC: a prospective study. Int J Radiat Oncol Biol Phys 71: 1402-1407.
15. International Atomic Energy Agency (IAEA), Nuclear Medicine Section 2008 The role of PET/CT in radiation treatment planning for cancer patient treatment IAEA-TECDOC-1603 Vienna: IAEA.
16. Xing L, Cotrutz C, Hunjan S, Boyer AL, Adalsteinsson E, et al. (2002) Inverse planning for functional image-guided intensity-modulated radiation therapy. Phys Med Biol 47: 3567-3578.
17. Das S K, Miften M M, Zhou S, Bell M, Munley MT, et al. (2004) Feasibility of optimizing the dose distribution in lung tumors using ? uorine-18-?uorodeoxyglucose positron emission tomography and single photon emission computed tomography guided dose prescriptions. Med Phys. 31 :1452-1461
18. Vanderstraeten B, Duthoy W, De Gersem W, De Neve W, Thierens H (2006) [18F]fluoro-deoxy-glucose positron emission tomography ([18F]FDG-PET) voxel intensity-based intensity-modulated radiation therapy (IMRT) for head and neck cancer. Radiother Oncol 79: 249-258.
19. Duprez F, De Neve W, De Gersem W, Coghe M, Madani I (2011) Adaptive dose painting by numbers for head-and-neck cancer. Int J Radiat Oncol Biol Phys 80: 1045-1055.
20. Yang Y, Xing L (2005) Towards biologically conformal radiation therapy (BCRT): selective IMRT dose escalation under the guidance of spatial biology distribution. Med Phys 32: 1473-1484.
21. Sánchez-Crespo A, Andreo P, Larsson SA (2004) Positron flight in human tissues and its influence on PET image spatial resolution. Eur J Nucl Med Mol Imaging 31: 44-51.
22. Sánchez-Crespo A, Larsson SA (2006) The influence of photon depth of interaction and non-collinear spread of annihilation photons on PET image spatial resolution. Eur J Nucl Med Mol Imaging 33: 940-947.
23. Sanchez-Crespo A (2013) Comparison of Gallium-68 and Fluorine-18 imaging characteristics in positron emission tomography. Appl Radiat Isot 76: 55-62.
24. South CP, Evans PM, Partridge M (2009) Dose prescription complexity versus tumor control probability in biologically conformal radiotherapy. Med Phys 36: 4379-4388.
25. Meijer G, Steenhuijsen J, Bal M, De Jaeger K, Schuring D, et al. (2011) Dose painting by contours versus dose painting by numbers for stage II/III lung cancer: practical implications of using a broad or sharp brush. Radiother Oncol 100: 396-401.
26. Tomasi C, Manduchi R (1998) Bilateral Filtering for Gray and Color Images Proceedings of the 1998 IEEE. International Conference on Computer Vision, Bombay, India
27. Otsu N (1979) A threshold selection method from gray-level histograms IEEE Transactions on Systems, Man, and Cybernetics. SMC 9 :62-66.
28. Nahum AE, Sanchez-Nieto B (2001) Tumour control probability modeling: Basic principles and applications in treatment planning. Physica Medica 17 : 13-23.
29. Wyatt RM, Jones BJ, Dale RG (2008) Radiotherapy treatment delays and their influence on tumour control achieved by various fractionation schedules. Br J Radiol 81: 549-563.
30. Webb S (1994) Optimum parameters in a model for tumour control probability including interpatient heterogeneity. Phys Med Biol 39: 1895-1914.
31. Stuschke M, Thames HD (1999) Fractionation sensitivities and dose-control relations of head and neck carcinomas: analysis of the randomized hyperfractionation trials. Radiother Oncol 51: 113-121.
32. Uzan J, Nahum AE (2012) Radiobiologically guided optimisation of the prescription dose and fractionation scheme in radiotherapy using BioSuite. Br J Radiol 85: 1279-1286.
33. Emami B, Lyman J, Brown A, Coia L, Goitein M, et al. (1991) Tolerance of normal tissue to therapeutic irradiation. Int J Radiat Oncol Biol Phys 21: 109-122.
34. Marks LB, Yorke ED, Jackson A, Ten Haken RK, Constine LS, et al. (2010) Use of normal tissue complication probability models in the clinic. Int J Radiat Oncol Biol Phys 76: S10-19.